SAND2022-1775J

Deciphering the influence of high-flux helium plasma exposure on tungsten nanostructure growth using real-time, in-situ spectroscopic ellipsometry

Robert D. Kolasinski[a,*], Chun-Shang Wong[a], Aaron Engel[a,†], Josh A. Whaley[a], Frances I. Allen[b], and Dean A. Buchenauer[a]

[a]*Sandia National Laboratories, Plasma and Reacting Flow Science Department, Livermore, CA 94550 USA*

[b]*University of California, Berkeley, Department of Materials Science & Engineering, Berkeley, CA 94720 USA*

ABSTRACT

In-situ analysis of surfaces during high-flux plasma exposure represents a long-standing challenge in the study of plasma-material interactions. While post-mortem microscopy can provide a detailed picture of structural and compositional changes, in-situ techniques can capture the dynamic evolution of the surface. In this study, we demonstrate how spectroscopic ellipsometry can be applied to real-time characterization of W nanostructure (also known as "fuzz") growth during exposure to low temperature, high-flux He plasmas. Strikingly, over a wide range of sample temperatures and helium fluences, the measured ellipsometric parameters (Ψ, Δ) collapse onto a single curve that can be directly correlated with surface morphologies characterized by ex-situ helium ion microscopy. The initial variation in the (Ψ, Δ) parameters appears to be governed by small changes in surface roughness (< 50 nm) produced by helium bubble nucleation and growth, followed by the emergence of 50 nm-diameter W tendrils. This basic behavior appears to be reproducible over a wide parameter space, indicating the spectroscopic ellipsometry may be of general practical use as a diagnostic to study surface morphologies produced by high-flux He implantation in refractory metals. An advantage of the methods outlined here is that they are applicable at low incident ion energies, even below the sputtering threshold. As an example of this application, we apply in-situ ellipsometry to examine how W fuzz growth is affected both by varying ion energy as well as the temperature of the surface.

I. INTRODUCTION

Understanding and predicting how materials respond to high-flux plasma exposure is crucial for many applications within plasma science, especially within the field of nuclear fusion. In addition to hydrogen isotopes, fusion edge plasmas potentially contain smaller quantities of He, sputtered and desorbed impurities from the surrounding wall materials, as well as deliberately introduced species (typically N, B, or Ne). These particles are predominantly low energy (< 100 eV) and are implanted into the first few nm of the exposed interface, and nucleate defects within a narrow region (~ 50 nm)

[*]Corresponding author (R. Kolasinski):
email: rkolasi@sandia.gov
address: Sandia National Laboratories, P.O. Box 969, MS 9161, Livermore, CA, 94550 USA
PH: +1 (925) 294-2872

[†]Present affiliation: University of California, Santa Barbara, Department of Materials Science, Santa Barbara, CA 93117

near the surface [1]. In addition to these ions, higher energy charge-exchange neutral particles may also reach the plasma-exposed interface. The surface degradation caused by the plasma limits the practical material lifetime, but its effects are far broader. As the plasma continuously modifies surface structure, new defects are created which can also trap hydrogen isotopes [2]. For burning plasmas that rely on a mixture of tritium and deuterium, permeation of tritium through materials poses a radiological safety issue [3,4]. Furthermore, the effect of the reconstituted surface on edge plasma operation remains an open question. Unfortunately, current understanding of the coupled mechanisms underlying these effects falls far short of what is needed for reliable predictions of material lifetime and tritium retention in magnetic confinement fusion devices.

Our knowledge of these basic mechanisms could be advanced considerably with in-situ diagnostics capable of probing how surface composition and structure are modified by the plasma. However, a significant obstacle is that most established forms of electron-based spectroscopy and microscopy are incompatible with a plasma environment. One strategy for overcoming these problems includes transferring samples in-vacuum into characterization stations attached directly to the plasma device [5-8], or into a separate surface science instrument via a self-contained portable chamber [9]. This allows for intermittent characterization, providing information on a "shot by shot" basis. Alternatively, better time resolution can be realized through in-situ optical and laser-based techniques. Examples include laser-induced breakdown spectroscopy (LIBS) [10] and laser-induced desorption spectroscopy (LIDS) [11], which allow for analysis of surface composition and hydrogen isotope retention. High energy ion beam analysis offers an avenue for probing the depth distribution of implanted species in-situ [12]. Another noteworthy recent development is in-situ TEM, which allows for direct imaging of nm-sized bubble nucleation and growth [13]. To date, this technique has been restricted to low-flux ion bombardment but has the potential to provide unique insight into defect formation and bubble migration.

While the in-situ techniques described above provide valuable insight into mechanisms governing surface modification by plasmas, they do not measure how the surface morphology evolves. In-situ spectroscopic ellipsometry presents an intriguing method of capturing this information. The technique is non-destructive (and non-contact), is not dependent on the absolute reflectivity of the surface and provides sensitivity to nm-scale changes in roughness. To determine this information, ellipsometry measures how the polarization of light is changed when reflected from a sample surface. By measuring changes in polarization as opposed to changes in reflectivity, ellipsometry is more robust against instabilities in the experimental instrumentation, including variations in the beam intensity, and provides greater sensitivity to thin surface layers. While reflectometry has been successfully applied in quantifying degradation in the performance of diagnostic mirrors intended for use in nuclear fusion devices [14,15], ellipsometry could provide complementary information on surface roughening or coating with sputtered impurities due to exposure to the plasma environment. One limitation of this approach is that ellipsometry provides direct information only on the optical properties of the surface, rather than on its physical structure. As a result, an understanding of the basic surface configuration and its composition is required in order to quantitatively interpret the results. Fortunately, this is usually possible through comparisons with microscopy or surface science techniques (e.g. Auger electron spectroscopy coupled with ion beam depth profiling). Modelling the ellipsometry results also often presents challenges for complex surface morphologies; different approaches are discussed in Sect. III of this article.

The application of ellipsometry for in-situ study of plasma-surface interactions was previously explored by Bastasz and co-workers [16]. In that work, a single wavelength ellipsometer was attached to the PISCES-B linear plasma device and successfully measured the erosion rate of a SiO_2 film on a Si substrate during D_2^+ plasma bombardment. While many of the practical issues associated with implementing in-situ ellipsometry on a large plasma device were identified and solved, the work of Bastasz et al. addressed only very modest changes to the surface (erosion of only ~5 nm). Miyamoto [17] and Nishijima [18] later relied on ex-situ ellipsometry to observe differences in optical features of tungsten exposed to He plasmas as compared with pristine surfaces over wavelengths of 200 nm – 900 nm. These results demonstrated that it is plausible to also extract meaningful information from the wavelength dependence of the refractive index and extinction coefficients determined by

ellipsometry. An open question is whether such an approach could be applied in-situ to a broader range of problems for fusion plasmas.

In this article, we extend the use of in-situ spectroscopic ellipsometry to study complex surface morphology changes driven by plasma exposure in real time. In this case, we consider the W+He model system, where high-flux helium plasma exposure of W leads to the growth of a layer of nanotendrils, also known as tungsten "fuzz". Here, we correlate the optical properties of the surface, as determined by in-situ ellipsometry, to changes in surface morphology using ex-situ microscopy. We find that the ellipsometry measurements are sensitive to the fuzz layer thickness for experimental conditions relevant for fusion applications. For this study, this encompasses temperatures ranging between 472 – 937 °C, ion energies < 250 eV, and particle fluences up to 1.2×10^{25} m^{-2}. Our initial objective with this work is to demonstrate the use of in-situ ellipsometry as a diagnostic for fundamental studies of early-stage effects of He on plasma-facing materials. Data on fuzz layer thickness and its rate of growth under different exposure conditions is valuable information that can help motivate modelling studies. Beyond this, we envision that the in-situ ellipsometry approach discussed here could be applied to a variety of plasma-material interactions studies in linear plasma devices. This approach, coupled with other characterization tools, could eventually be used to measure erosion and redeposition of thin films as well as surface morphology changes.

The W+He model system is particularly important in the realm of plasma-material interactions in fusion devices. Tungsten will be used in the divertor of ITER, an international magnetic-confinement fusion experiment under construction in Cadaraché, and is a leading option for wall materials in many demonstration reactor concepts. During high-flux, low energy plasma exposure, He can nucleate a dense layer of nm-sized bubbles within the first ~50 nm of the surface. At higher temperatures, these effects become more pronounced, creating surface ripples, and eventually a layer of ~50 nm diameter tendrils. Fig. 1 shows the evolution of these surface features with increasing fluence. The individual images depict nanostructure layers with thicknesses of 135 nm, 180 nm, and 350 nm following exposure to He fluences of $\Phi_{ion} = 1.4\times10^{24}$ m^{-2}, 4.3×10^{24} m^{-2}, and 7.2×10^{24} m^{-2}, respectively. Despite the considerable experimental and theoretical work that has been invested in exploring this system over the past 10 years since its discovery [19-21], the mechanisms underlying its growth are debated, and a comprehensive model has remained elusive. A summary of mechanisms proposed by different researchers appears in Hammond's recent review [22] and include: (a) bubble growth and rupture, (b) dislocation and grain boundary segregation, (c) void-coalescence, (d) electric-field induction, and (e) sputtering and (selective) erosion. As pointed out by Hammond, there appears to be consensus that bubble growth and rupture is clearly one of the main drivers for nanostructure growth, while mechanisms (c) – (e) have fallen out of favor due to a lack of supporting experimental evidence. The importance of near-surface He bubble growth to surface roughening in the initial stages of plasma exposure has been highlighted in several recent experimental [23] and modelling studies [24-26]. Setting aside the lack of consensus on some of the other underlying mechanisms, predicting the evolution of these surface morphologies is of considerable practical importance. Exfoliation of the damaged surface could be a significant impurity source within core fusion plasmas, and near-surface He precipitation is known to dramatically affect tritium trapping and permeation [2].

II. EXPERIMENTAL METHODS

The RF plasma source used for this work consists of a 2 m long cylindrical vacuum vessel (25 cm dia.) constructed from stainless steel UHV components. The chamber itself is equipped with a turbomolecular pump, enabling an ultimate base pressure of 6.5×10^{-6} Pa (5×10^{-8} Torr) to be reached. Four magnet coils positioned along the length of the chamber produce an axial magnetic field. A cylindrical He^{+} plasma discharge, approximately 5 cm in diameter, is generated by applying RF power to a slotted Cu coil located inside the chamber. The coil design is based on prior work by Lisitano [27, 28], with later refinements by Kerst [29, 30], and is intended to direct electromagnetic waves along its axis and ionize the neutral gas using a non-resonant process (frequency: 420 MHz.) Under typical conditions, we operate the source with an applied axial magnetic field of 185 G, RF power of 250 W,

and He neutral pressure of 0.65 Pa (5 mTorr.) A Langmuir single probe attached to a linear translation stage allows measurement of the plasma parameters at different radial positions within the plasma column. The incident ion flux reached a peak of 4.0×10^{20} $m^{-2}s^{-1}$ under normal operating conditions. Further information on the fitting and modelling approach for the Langmuir probe data are described in Ref. [31].

Control of impurities within the plasma is an important consideration for these measurements. To minimize sputtering from heavier gas-phase impurities (O and N), we pumped out and purged the He gas lines prior to each experiment. We also relied on a gas purity sensor to check for any changes in the gas composition. In addition, we measured the mass of specimens before and after plasma exposure to confirm that sputtering was negligible. One potential problem with having the Lisitano coil inside the plasma chamber is the possibility of sputtering and redeposition on sample surfaces. We anticipated that this would not be a serious problem, given that the coil is grounded, the plasma potential is small (~40 eV), and the ion temperature of the plasma is also low. To verify our assumptions, we characterized the W specimens looking for signs of Cu, Fe, and other deposited impurities using x-ray photoelectron spectroscopy (XPS) and Auger electron spectroscopy (AES). Aside from chemisorbed O and C (very typical following exposure to air), we found no evidence of other impurities. There was also no evidence of sputter-deposited Ta from the front mask used to secure the specimen to the target holder. The sensitivity of our AES and XPS instruments is approximately 0.5% at.

Because ellipsometry is sensitive to differences in surface morphology, consistency of sample fabrication and surface preparation is an important consideration. For this work, specimens were cut from polycrystalline W (ITER-grade [32], Allied Materials Corporation) via electrical discharge machining and mechanically polished to an RMS surface finish of 10 nm. The spot size from the beam of the ellipsometer required the use of 25 mm diameter specimens (2 mm thick) for in-situ analysis. For ex-situ analysis, smaller 6 mm diameter buttons were used for convenience. After polishing, all samples were heated to 900 °C in an ultra-high vacuum (UHV) furnace (< 10^{-7} Torr) over a 30 min. interval and held at this temperature for 1 hr. Prior electron backscatter diffraction measurements on these materials indicate that the grains range between 10 – 20 μm in width [33]. In addition to the ITER-grade specimens, one sample of rolled polycrystalline W (Goodfellow) was also included in our test matrix for comparison.

Following annealing, the W specimens were then mounted to a target equipped with a button-style heater, enabling sample temperatures up to 1000 °C to be reached. The sample temperature was measured using a type C thermocouple spot-welded to a Ta foil placed beneath the sample. Because the thermocouple may pick up some current from the plasma (thereby distorting the signal), we also used an optical pyrometer to monitor the stability of the sample temperature during exposure. The samples were isolated from the heater using a sapphire disc, allowing the collected ion current to be measured. For most of the exposures discussed here, the applied bias was -50 V relative to the chamber ground. When corrected for the plasma potential (42 eV), the resulting calculated ion energy was 92 eV. For the He plasmas considered here, we did not note any appreciable mass loss for the samples exposed to plasmas at a bias of -125 V (ion energy: 167 eV.) The temperature range and incident ion flux encompass the conditions required for He-induced nanostructure growth.

Following plasma exposure, all specimens were imaged using a helium ion microscope (HIM), the Zeiss ORION NanoFab. This was used to assess how the surface morphology changed after exposure. In cases where plasma exposure had produced a thick fuzz layer, we determine its thickness with Ga^+ focused ion beam (FIB) profiling. Because of the delicate nature of the nano-tendrils, care was taken to use a low beam current for the FIB milling and the beam scanning parameters were tuned to produce clean cuts free from redeposited material. Using a 25 keV Ga^+ beam at 10 pA, a rectangular area of dimensions 3 μm × 3 μm was first milled using standard raster scan mode to a depth of approximately 1 μm. Then, reducing to 1 pA, the final cleaning cuts of the cross section were performed using a reduced rectangle of dimensions 3 μm × 100 nm, with the long side of the rectangle closest to the region of interest milled last. This final rectangle was milled using a scanning mode in which each scan line is milled multiple times before moving on to the next line, rather than the many repeats across the same area that are performed in raster scan mode. Each cross section was then

imaged by HIM under an angle of 54 degrees relative to the surface normal. The HIM images were acquired using a 1-2 pA He^+ beam (beam diameter ~ 0.5 nm) at 25 keV. There was no discernible change in the sample morphology resulting from the HIM imaging. In cases where the morphology was in its early stage of formation, we used atomic force microscopy to generate surface height maps.

For in-situ measurements, a spectroscopic ellipsometer (245 – 1000 nm wavelength range) was attached to the RF-plasma source with direct line-of-sight to the sample surface, as shown in Fig. 2. Both the ellipsometer light source and detector were mounted to gimbals and aligned to a specular angle of 70°. Following installation and alignment, we calibrated the ellipsometer using a 25 nm SiO_2 layer grown on a Si substrate to precisely determine the offsets for the ellipsometer polarizers and any errors introduced by the optical viewports. To allow us to compensate for thermal expansion, the sample stage was equipped with a micrometer positioner. During each exposure, complete ellipsometry spectra were acquired every 2 s.

III. RESULTS AND DISCUSSION

Fig. 3 shows results from in-situ ellipsometry measurements, as indicated by the three solid curves corresponding to exposure times of 1 hr, 3 hrs, and 5 hrs. Here the data are rendered in terms of the two parameters measured by the ellipsometer, Ψ and Δ, used to determine the polarization change of the reflected light. The phase difference between the parallel and perpendicular components of the incoming and outgoing light are indicated by δ_i and δ_o, respectively. The parameter $\Delta = \delta_i - \delta_o$ is the phase shift that occurs upon reflection and can have any value between 0 - 360°. Amplitude information, on the other hand, is contained in the parameter Ψ, which ranges between 0-90°. It is related to the ratio of the magnitudes of the parallel and perpendicular components of the total reflection coefficients, (denoted as r_p and r_s, respectively), by $\tan(\Psi) = |r_p|/|r_s|$. These two basic quantities can be combined to give the complex ratio ρ of total reflection coefficients by the expression below:

$$\tan(\Psi)\, e^{i\Delta} = \rho = r_p/r_s$$

While the ellipsometer collected data over its entire spectral range, three discrete wavelengths (245 nm, 624 nm, and 999 nm) are shown in Fig. 3 for simplicity. Except for the total plasma fluence, the exposure conditions were identical for each of the in-situ measurements (E_{ion} = 92 eV, $T_{surface}$ = 900 °C, and $\Gamma_{ion} = 4.0\times10^{20}$ m^{-2} s^{-1}). The three exposures correspond to the same images depicted in Fig. 1. The in-situ data trace out different lengths along the same trajectory in (Ψ, Δ) space. This illustrates not only the reproducibility of the experimental conditions and measurement technique, but also that of the He bubble nucleation and fuzz growth process. There is a slight variability in the values of (Ψ, Δ) for each sample at $t = 0$, which we attribute to small variations in surface preparation (e.g. small differences in oxidation and surface roughness).

-Table 1: Summary of ex-situ data sets for low energy He^+ exposure of W surfaces

data set ID	# of samples	Comments
A	9	Sample temperature varied between 472 – 937 °C. Exposure conditions: E_{ion} = 92 eV; $\Gamma_{ion} = 4.0\times10^{20}$ m^{-2} s^{-1}; $\Phi_{ion} = 7.2\times10^{24}$ m^{-2}. Material: ITER-grade W
B	6	Ion fluence varied between $\Phi_{ion} = 5.0\times10^{23} – 1.2\times10^{25}$ m^{-2}. Exposure conditions: T_{sample} = 840 °C; E_{ion} = 92 eV; $\Gamma_{ion} = 2.7\times10^{20}$ m^{-2} s^{-1}. Results reported in Ref. [26]. Material: ITER-grade W
C	1	Exposure conditions: T_{sample} = 900 °C; E_{ion} = 92 eV; $\Gamma_{ion} = 4.0\times10^{20}$ m^{-2} s^{-1}, $\Phi_{ion} = 7.2\times10^{24}$ m^{-2}. Material: rolled polycrystalline W foil
D	5	Exposure conditions: T_{sample} = 840 °C; E_{ion} = 92 eV; $\Gamma_{ion} = 4.0\times10^{20}$ m^{-2} s^{-1}; $\Phi_{ion} = 8.6\times10^{24}$ m^{-2}. Material: ITER-grade W. Results reported in Ref. [31].

While several factors influence the ellipsometry measurements described here, the most important contribution is the dramatic roughening of the surface depicted in the images in Fig. 1. This effect has been well documented, particularly in prior work by Aspnes and co-workers [37]. To better understand how changes in the (Ψ, Δ) trajectories are correlated to surface morphology, we performed ex-situ characterization of 21 additional tungsten samples exposed to pure He^+ plasmas over a wide range of temperatures and fluences. The exposure conditions for these samples are summarized in Table 1, with further details included in Refs. [26, 34] and in the supplemental online information. After plasma exposure, we acquired ex-situ ellipsometry spectra for each specimen and imaged its surface morphology using helium ion microscopy (HIM). The thickness of the fuzz layer was also determined by gallium focused ion beam profiling. The (Ψ, Δ) values for each sample are indicated in Fig. 3 by markers for the same 70° specular reflection angle used for the in-situ measurements. The corresponding thicknesses of the nanostructure layer for select specimens exposed at varying temperatures (series "A" in Table 1) are indicated in units of nm in the figure overlay. For comparison, the final thickness of the fuzz layer measured for the in-situ samples is also indicated using the red labels. Though these data were acquired over a wide range of conditions, it is striking that they all appear to collapse onto a single curve in (Ψ, Δ) space, tracing out a trajectory that depends on the fuzz layer thickness. Taking the 624 nm case as an example, changes in Δ span over 120°, whereas Ψ varies over 12° as the nanostructure thickness approaches 1 μm. These changes are far larger than the uncertainty introduced by small variations in surface preparation.

There are several unusual features of the plots shown in Fig. 3 that are worth considering. First, a sharp "knee" in the data is present $\lambda = 245$ nm as the fuzz layer thickness reaches between 360 – 405 nm. This same knee is less prominent in the $\lambda = 624$ nm plot and absent from the $\lambda = 999$ nm. This suggests a connection between the wavelength of light used to probe the surface and the fuzz thickness, though more modelling is needed to understand the precise mechanism. As for the shapes of the trajectories, changes in Δ and Ψ themselves do not provide much physical insight without being correlated with microscopy, as these two parameters are only the raw data that is measured by the ellipsometer. In principle, an alternate approach involves using the Δ and Ψ values to calculate the "effective" index of refraction $\langle n \rangle$ and extinction coefficient $\langle k \rangle$. Such results must be interpreted with care, however, as changes in roughness can produce similar effects to changes in refractive index and extinction coefficient. In this case, (Ψ, Δ) trajectories appeared to be a more straightforward way to interpret the data.

To demonstrate that our ellipsometry results were insensitive to the sample temperature, we performed two further sets of in-situ measurements. These measurements were intended to address any concerns that changes to the emissivity of the W surface or desorption of impurities due to heating may have led to differences between our ex-situ and in-situ results, which were obtained at room temperature and at temperatures as high as 900 °C, respectively. First, to determine the significance of this issue, we measured changes in Ψ and Δ during heating of a pristine, unexposed sample to 900 °C and cooling afterward. As described in the supplemental information, in the most severe cases, Δ varies only by 4°, whereas Ψ changes by 1°. This indicates that changes in the emissivity are not drastically affecting the measured results; in fact, these variations are far smaller than the observed changes resulting from fuzz growth discussed here. As further support of this, consider the in-situ data shown in Fig. 4(a). Here, data was obtained for exposure temperatures of 720 °C and 900 °C and, as is evident from the plot, the two data sets nearly overlap. The 900 °C case traces out a longer trajectory due to more extensive fuzz growth. These results provide evidence that even at elevated temperature, ellipsometry is a robust diagnostic of He-induced surface morphologies.

The agreement between the in-situ and ex-situ measurements is satisfactory, but it was initially unclear why these data collapse onto a single (Ψ, Δ) trajectory, given the broad range of exposure conditions. A qualitative inspection of the images in Fig. 1, as well as in Refs. [26, 31], shows that the characteristic lateral size of the surface features generated by He plasma exposure are within the range of 50 – 100 nm. A more quantitative analysis is possible at the initial stages of fuzz growth by using atomic force microscopy (AFM) to map surface roughness. As described in our prior work (in collaboration with Dasgupta et al., c.f. Ref. [26]), the lateral dimensions measured by AFM for several W specimens exposed to low He fluence fall within the range mentioned above. This suggests that,

over the parameter space explored here, the dimensions of the structures created by He plasma exposure are similar, with changes in exposure temperature mainly serving to accelerate or decelerate the growth process.

A fundamental question is: Under what circumstances would the results deviate from this behavior? One parameter that we have not varied until now is the incident ion energy, which has been kept consistent between tests at 92 eV. In Fig. 4(b), in-situ data are shown for ion energies of 92 eV, 167 eV, and 542 eV, with corresponding HIM images in panels (c) and (d). All exposures were performed at the same temperature (900 °C) and plasma flux (4.0×10^{20} m^{-2} s^{-1}.) For comparison, a specimen exposed at 92 eV under the same conditions appears in Fig. 1. Unlike previous cases, the higher energy exposures deviate considerably from the previously established pattern, suggesting differences in the evolution of the fuzz layer. Whereas exposure at 167 eV results in a thicker nanostructure layer (c.f. Fig. 4(c)), increasing the particle energy to 542 eV appears to impede the growth of the nanotendrils. A plausible explanation for this phenomenon is that below the sputtering threshold, increasing the incident ion energy results in more He implantation into the lattice, thereby accelerating bubble nucleation and growth. Fuzz growth can proceed if the ion energy is kept sufficiently low so that sputtering is not appreciable. This appears to be true for our exposures at 92 eV and 167 eV. At higher energies, sputtering by He^+ ions become increasingly important, as in the 542 eV case. From the HIM image in Fig. 4(d), clearly erosion begins to compete with fuzz growth at this energy, consistent with prior experimental work [35] and modelling [36]. In either case, the difference in surface structure is easily detectable by ellipsometry.

To better understand the information contained in the ellipsometry measurements, it is useful to consider different ways to model how roughness affects the ellipsometry result itself. Fitting the ellipsometry data and modelling these results is a topic of active investigation and will be reported in a future study. An overview of the general approach is provided here. One important consideration is the average feature size relative to the wavelength of light used in the ellipsometry analysis, λ. Some guidance on this topic can be found in prior work by Aspnes [37]. During the initial stages of fuzz growth, the surface roughness is rather modest, with the variations in surface height < 50 nm. Under such conditions, even in the UV range, the surface feature size is $\ll \lambda$. Here, it is reasonable to employ the "effective medium" approach detailed in Ref. [37] to model the ellipsometry data. This involves approximating the surface roughness with a thin layer that has been reduced in density. As surface features grow, a "graded medium" approximation as described in prior work by Lehmann et al. [38] may be used to account for density gradients in the early-stage fuzz growth. Here atomic force microscopy surface height maps could be used to provide layer density as a function of thickness. In principle, a combination of these two approaches could be used to provide insight into the surface morphology as it evolves. As the surface feature size (e.g. the tendril length or fuzz thickness) approaches the wavelength of light used in the ellipsometry analysis, the assumptions used in these models may begin to break down. Under such conditions, scattering and depolarization of the incident light may begin to dominate the measurement. Even with this limitation, one can still empirically compare the observed structures with the ellipsometry results to provide insight into the surface morphology.

IV. CONCLUDING REMARKS AND OUTLOOK

A primary goal of this study was to test the effectiveness of spectroscopic ellipsometry as an in-situ diagnostic for the effects of He plasmas on W surfaces. Because ellipsometry is highly sensitive to nm-scale changes in surface roughness, it can capture initial surface morphologies produced by the He plasma that typically only can be detected using microscopy. The contribution of nanoscale surface features to the measured ellipsometry signal easily overwhelms the influence of secondary effects such as surface preparation and sample temperature. This enabled us to obtain reliable measurements from room temperature up to 900 °C. Furthermore, if the incident plasma flux and fluence can be adequately controlled, the nanostructure growth is highly reproducible, making it possible to develop an adequate database of ex-situ microscopy to calibrate against the ellipsometry

measurements. Using this approach is was possible to measure the thickness of the tungsten fuzz layer over a range 77 nm – 900 nm. For these reasons, ellipsometry appears to be well-suited for fundamental studies of He+W interactions, and in particular for investigations of early-stage tungsten nanostructure growth.

Over a wide range of exposure parameters, the He-induced surface morphologies conform to a single trajectory in (Ψ, Δ) space. This indicates that the fundamental way in which the plasma modifies the surface remains similar over the parameter space examined here, with increases in temperature serving mainly to accelerate the surface morphology evolution. We also demonstrated the ability to identify different sputtering regimes depending on the energy of the incident ions. Further progress may be possible through modeling the ellipsometric results. During the initial stages of plasma exposure, the average surface feature size (i.e., the mean height and correlation length) is much smaller than the wavelength of light used to probe the surface. For such cases, "effective medium" [37] or "graded medium" approximations [38] can be correlated with microscopy and fitted to the ellipsometry data. This is a topic of ongoing research and will be reported in future work.

From a practical standpoint, our work did not find major obstacles to applying ellipsometry to other linear plasma devices for in-situ measurements. The main constraint is the need for direct optical line-of-sight access to the sample. If this is not possible, the use of mirrors or other optical components would be required, as well as calibration to account for changes in the ellipsometric angles due to reflections. While the relatively modest magnetic fields present in our RF-plasma source did not pose any issues for our ellipsometer, the higher fields in some larger plasma devices may affect the operation of motorized components. These effects can usually be mitigated through shielding or other countermeasures. Because the integration time for ellipsometry is relatively short (in this case, about 2 s per measurement), we believe it would be possible to operate at higher plasma fluxes. Even if the nanostructure growth rate were an order of magnitude higher than what we encountered in our experiments, the integration time should not be a serious limitation in resolving the fuzz growth.

Implementation on a larger device such as a tokamak would present more significant challenges from a practical standpoint. Availability of appropriate sightlines to the surface for characterization may be limited, and some form of in-situ calibration and alignment would be needed. Alternatively, the technique could be quite effective on a short pulse device where samples could be exposed and retracted in-vacuuo into a secondary analysis chamber afterward. Measurements obtained between could then provide valuable information on surface morphology changes. Under such conditions, the potential for ellipsometry, in combination with other techniques, to yield insight into erosion/redeposition studies and effects of impurities on plasma-exposed surfaces appears particularly promising.

SUPPLEMENTARY MATERIAL

Additional information on helium plasma exposure conditions and the effects of temperature on the ellipsometry measurements is contained in the online supplementary material.

ACKNOWLEDGEMENTS

It is a pleasure to thank Robert Bastasz for helpful discussions which provided the motivation for this work. In addition, we express our appreciation to Andrew Shone (University of Illinois) for designing the Langmuir probe used in this study. We also are indebted to Paul Lum (University of California, Berkeley) and the Biomolecular Nanotechnology Center (BNC) for providing access to the HIM. This work was supported through the U.S. Department of Energy Office of Fusion Energy Sciences, through the Fusion Materials program. Sandia National Laboratories is a multimission laboratory managed and operated by National Technology and Engineering Solutions of Sandia LLC, a wholly owned subsidiary of Honeywell International Inc. for the U.S. Department of Energy's National Nuclear Security Administration under contract DE-NA0003525.

AUTHOR DECLARATIONS

The authors have no conflicts to disclose.

DATA AVAILABILITY

The data that support these findings of this study are available from the corresponding author upon reasonable request.

FIGURE CAPTIONS

Fig. 1: Helium ion microscope images showing the growth of ~50 nm diameter W tendrils following He^+ plasma exposure. The upper panels show a top view, whereas the lower panels include profile images produced using a focused gallium ion beam. Exposure conditions: T_{sample} = 900 °C; E_{ion} = 92 eV; $\Gamma_{ion} = 4.0\times10^{20}$ m^{-2} s^{-1}.

Fig. 2: Experimental diagram showing the in-situ configuration with the attached ellipsometer.

Fig. 3: (Ψ, Δ) plots for W surfaces exposed to varying He plasma conditions. In-situ measurements are given by the solid curves, which trace out a similar trajectory in (Ψ, Δ) space. For comparison, ex-situ spectroscopic ellipsometry measurements for 21 samples are indicated by markers. The fuzz layer thicknesses were measured via HIM for a subset of the samples and are indicated in nm by the labels next to each marker. The black labels correspond to samples where the ellipsometry was performed ex-situ, whereas the red labels indicate the final fuzz thickness measured by HIM for the specimens used in the in-situ analyses.

Fig. 4: In-situ (Ψ, Δ) data showing the effect of varying (a) exposure temperature and (b) ion energy. Post-mortem HIM reveals the final surface morphologies for specimens exposed to ion energies of 167 eV and 542 eV, shown in Figs. (c) and (d). Plasma conditions: $\Gamma_{ion} = 4.0\times10^{20}$ m^{-2} s^{-1}; $\Phi_{ion} = 7.2\times10^{24}$ m^{-2}.

REFERENCES

[1] B. D. Wirth, K. Nordlund, D. G. Whyte, and D. Xu, *MRS Bull.* **36**, 216 (2011).

[2] M. J. Baldwin, R. P. Doerner, W. R. Wampler, D. Nishijima, T. Lynch, and M. Miyamoto, *Nucl. Fusion* **51**, 103021 (2011).

[3] M. Shimada and C. N. Taylor, *Nucl. Mater. Energy*, **19**, 273 (2019).

[4] R. A. Causey, J. N. Brooks, and G. Federici, *Fus. Eng. Design* **61-62**, 525 (2002).

[5] Ch. Linsmeier, B. Unterberg, J. W. Coenen, R. P. Doerner, H. Greuner, A. Kreter, J. Linke, and H. Maier, *Nucl. Fusion* **57**, 092012 (2017).

[6] Y. Hirooka, R. W. Conn, T. Sketchley, W. K. Leung, G. Chevalier, R. Doerner, J. Elverum, D. M. Goebel, G. Gunner, M. Khandagle, B. Labombard, R. Lehmer, P. Luong, Y. Ra, L. Schmitz, and G. Tynan, *J. Vac. Sci. Technol. A* **8**, 1790 (1990).

[7] C. N. Taylor, B. Heim, S. Gonderman, J. P. Allain, Z. Yang, R. Kaita, A. L. Roquemore, C. H. Skinner, and R. A. Ellis, *Rev. Sci. Instrum.* **83**, 10D703 (2012).

[8] R. Kaita, M. Lucia, J. P. Allain, F. Bedoya, R. Bell, D. Boyle, A. Capece, M. Jaworski, B. E. Koel, R. Majeski, J. Roszell, J. Schmitt, F. Scotti, C. H. Skinner, and V. Soukhanovskii, *Fusion Eng. Des.* **117**, 135 (2017).

[9] A. Maan, R. Kaita, E. T. Ostrowski, R. Majeski, D. P. Boyle, D. C. Donovan, R. A. Ellis, B. E. Koel, and T. M. Biewer, *Rev. Sci. Instrum.* **91**, 026104 (2014).

[10] D. Nishijima, M. Patino, and R. P. Doerner, *Rev. Sci. Instrum.* **89**, 10J105 (2018).

[11] J. H. Yu, M. J. Baldwin, M. J. Simmonds, and A. Založnik, *Rev. Sci. Instrum.* **90**, 073502 (2019).

[12] G. M. Wright, H. A. Barnard, L. A. Kesler, E. E. Peterson, P. W. Stahle, R. M. Sullivan, D. G. Whyte, and K. B. Woller, *Rev. Sci. Instrum.* **85**, 023503 (2014).

[13] K. Hattar, D. C. Bufford, D. L. Buller, *Nucl. Instrum. Meth. B* **338**, 56 (2014).

[14] M. Sakamoto, T. Miyazaki, Y. Higashizono, et al. *Phys. Scr.* **T138**, 014043 (2009).

[15] M. Miyamoto, K. Ono, H. Urabe, et al. *Plasma Devices and Operations*, **17**, 155 (2009).

[16] R. Bastasz, Y. Hirooka, and M. Khandagle, *J. Nucl. Mater.* **220-222**, 352 (1995).

[17] M. Miyamoto, D. Nishijima, M. J. Baldwin, R. P. Doerner, Y. Ueda, K. Yasunaga, N. Yoshida, and K. Ono, *J. Nucl. Mater.* **415**, S657 (2011).

[18] D. Nishijima, R. P. Doerner, D. Iwamoto, Y. Kikuchi, M. Miyamoto, M. Nagata, I. Sakuma, K. Shoda, and Y. Ueda, *J. Nucl. Mater.* **434**, 230 (2013).

[19] S. Takamura, N. Ohno, D. Nishijima, and S. Kajita, *Plasma Fusion Res.* **1**, 051 (2006).

[20] S. Kajita, S. Takamura, N. Ohno, D. Nishijima, H. Iwakiri, and N. Yoshida, *Nucl. Fusion* **47**, 1358 (2007).

[21] M. J. Baldwin and R. P. Doerner, *Nucl. Fusion* **48**, 035001 (2008).

[22] K. D. Hammond, *Mater. Res. Express* **4**, 104002 (2017).

[23] K. Wang, R. P. Doerner, M. J. Baldwin, F. W. Meyer, M. E. Bannister, A. Darbal, R. Stroud, and C. M. Parish, *Sci. Rep.* **7**, 42315 (2017).

[24] K. D. Hammond, D. Maroudas, and B. D. Wirth, *Sci. Rep.* **10**, 2192 (2020).

[25] F. Sefta, K. D. Hammond, N. Juslin, and B. D. Wirth, *Nucl. Fusion* **53**, 073015 (2013).

[26] D. Dasgupta, R. D. Kolasinski, R. W. Friddle, L. Du, D. Maroudas, and B. D. Wirth, *Nucl. Fusion* **59**, 086057 (2019).

[27] G. Lisitano, R. A. Ellis Jr., W. M Hooke, and T. H. Stix, *Rev. Sci. Instrum.* **39**, 295 (1968).

[28] G. Lisitano, M. Fontanesi, and E. Sindoni, *Appl. Phys. Lett.* **16**, 122 (1970).

[29] R. A. Kerst, *J. Nucl. Mater.* **103 & 104**, 439 (1981).

[30] R. A. Kerst, *J. Vac. Sci. Technol.* **20**, 1267 (1982).

[31] C. -S. Wong, J. A. Whaley, T. Wada, S. Harayama, Y. Oya, and R. D. Kolasinski, *Nucl. Mater. Energy* **22**, 100730 (2020).

[32] ITER Materials Assessment Report, ITER Doc. G74 MA 10 01-07-11 W 0.2, 2001.

[33] R. D. Kolasinski, M. Shimada, Y. Oya, D. A. Buchenauer, T. Chikada, D. F. Cowgill, D. C. Donovan, R. W. Friddle, K. Michibayashi, and M. Sato, J. Appl. Phys. 118, 073301 (2015).

[34] R. D. Kolasinski, C. -S. Wong, A. Engel, J. A. Whaley, F. I. Allen, and D. A. Buchenauer, (in preparation.)

[35] Y. Noiri, S. Kajita, and N. Ohno, *J. Nucl. Mater.* **463**, 285 (2015).

[36] R. P. Doerner, M. J. Baldwin, and P. C. Stangeby, *Nucl. Fusion* **51**, 043001 (2011).

[37] D. E. Aspnes, J. B. Theeten, and F. Hottier, *Phys. Rev. B* **20**, 3292 (1979).

[38] D. Lehmann, F. Seidel, and D. R. T. Zhan, *Springer Plus* **3**, 82 (2014).

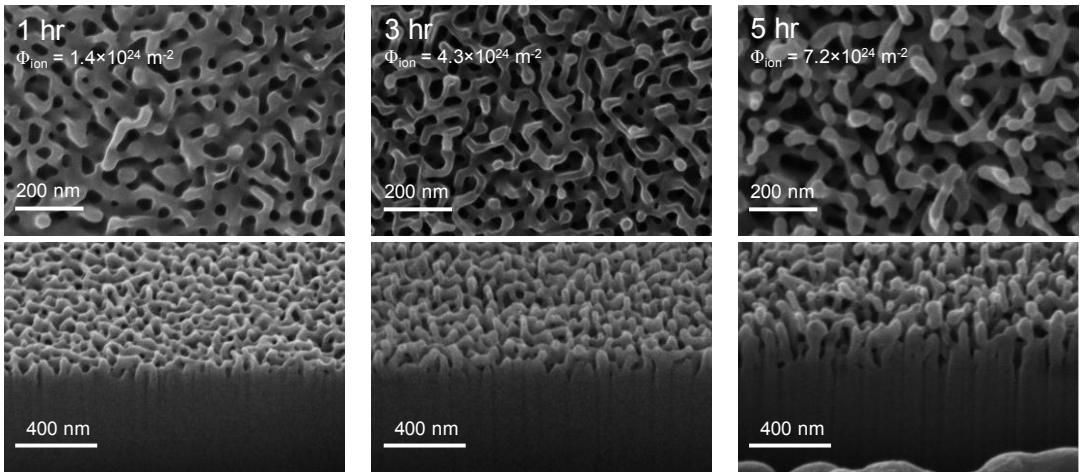

Fig. 1: Helium ion microscope images showing the growth of ~50 nm diameter W tendrils following He^+ plasma exposure. The upper panels show a top view, whereas the lower panels include profile images produced using a focused gallium ion beam. Exposure conditions: T_{sample} = 900 °C; E_{ion} = 92 eV; Γ_{ion} = 4.0×10^{20} m^{-2} s^{-1}.

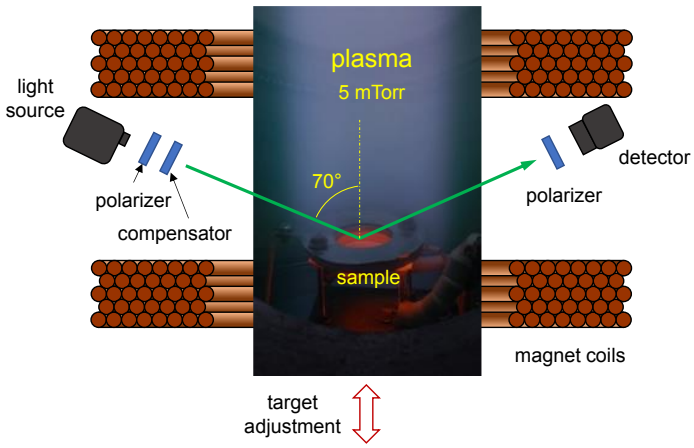

Fig. 2: Experimental diagram showing the in-situ configuration with the attached ellipsometer.

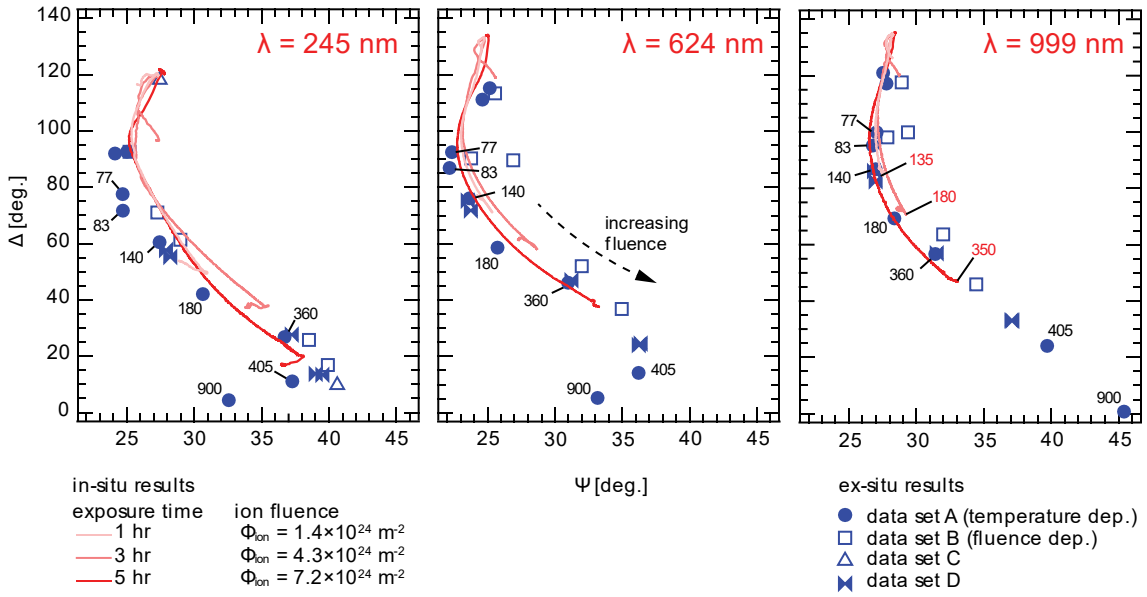

Fig. 3: (Ψ, Δ) plots for W surfaces exposed to varying He plasma conditions. In-situ measurements are given by the solid curves, which trace out a similar trajectory in (Ψ, Δ) space. For comparison, ex-situ spectroscopic ellipsometry measurements for 21 samples are indicated by markers. The fuzz layer thicknesses were measured via HIM for a subset of the samples and are indicated in nm by the labels next to each marker. The black labels correspond to samples where the ellipsometry was performed ex-situ, whereas the red labels indicate the final fuzz thickness measured by HIM for the specimens used in the in-situ analyses.

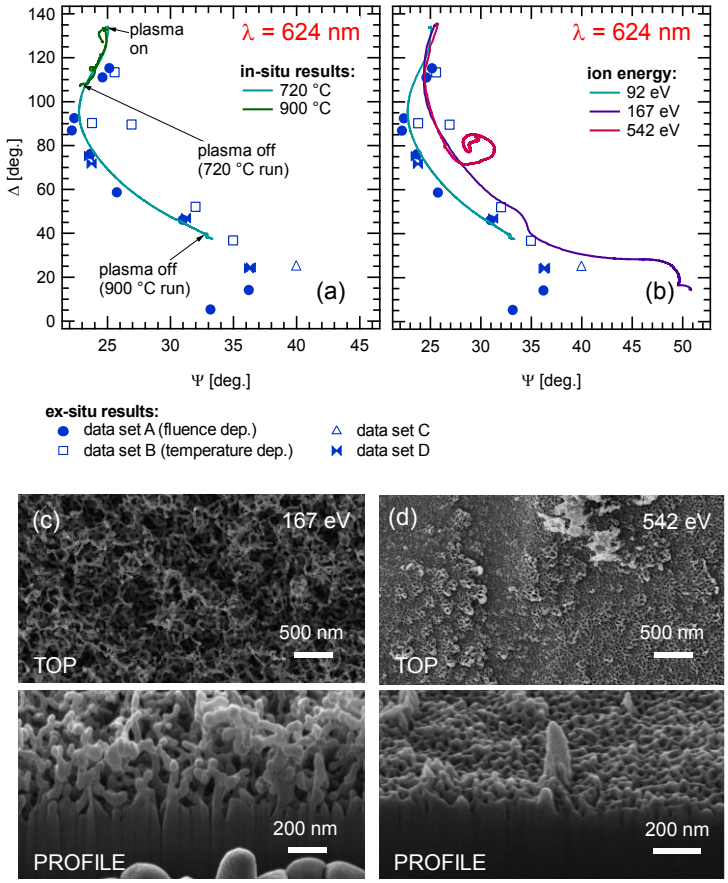

Fig. 4: In-situ (Ψ, Δ) data showing the effect of varying (a) exposure temperature and (b) ion energy. Post-mortem HIM reveals the final surface morphologies for specimens exposed to ion energies of 167 eV and 542 eV, shown in Figs. (c) and (d). Plasma conditions: $\Gamma_{ion} = 4.0\times10^{20}$ m^{-2} s^{-1}; $\Phi_{ion} = 7.2\times10^{24}$ m^{-2}.

Deciphering the influence of high-flux helium plasma exposure on tungsten nanostructure growth using real-time, in-situ spectroscopic ellipsometry

Robert D. Kolasinski[a,*], Chun-Shang Wong[a], Aaron Engel[a,†], Josh A. Whaley[a], Frances I. Allen[b], and Dean A. Buchenauer[a]

[a]*Sandia National Laboratories, Plasma and Reacting Flow Science Department, Livermore, CA 94551 USA*

[b]*University of California, Berkeley, Department of Materials Science & Engineering, Berkeley, CA 94720 USA*

SUPPLEMENTAL INFORMATION

I. Temperature Effects

To determine what effect changes in surface temperature have on the ellipsometry result, we measured the corresponding changes in Ψ and Δ for a pristine sample heated up to 900 °C and allowed to radiatively cool afterward, as illustrated in Fig. S1 for three wavelengths. Note that two identical heating cycles were performed on the sample, labelled as "cycle 1" and "cycle 2" in Fig. S1. These measurements were obtained in-situ using a button-style heater to heat the samples within the vacuum system for the RF source, without a plasma discharge. The heating cycle was terminated immediately after the samples reached 900 °C. In the most severe cases, Δ varies by as much as 4°, whereas Ψ changes by 1°. For the data acquired at wavelength of 245 nm, the starting point for the two cycles does not match. The most likely reason is a small amount of oxidation or segregation of impurities occurred during the intervening time. in any case, for the $He^+ \rightarrow W$ system under investigation here, these variations are far smaller than the observed changes resulting from nanostructure growth. These results provide evidence that, for our application, the effects of temperature will have only a modest effect on the interpretation of our measurements, thereby enabling one to obtain consistent results with ellipsometry even with W samples at elevated temperature. Accounting for such effects will pose a bigger challenge for systems where the surface is only modestly altered (e.g. removal of a thin oxide layer.)

II. Summary of Sample Exposure Conditions

A summary of four data sets (labelled "A" through "D") included in our ex-situ analyses appears in Table 1, in the main text of this article. More detailed information regarding the individual exposure conditions appears in Table S1, contained herein. Data set A examines the temperature dependence of He-induced surface morphology and nanostructure growth. A total of nine specimens were exposed at specific temperatures ranging between 472 – 937 °C in roughly 50 °C steps. Following exposure to plasma, the samples were imaged by HIM following the procedure described

*Corresponding author (R. Kolasinski):
email: rkolasi@sandia.gov
address: Sandia National Laboratories, P.O. Box 969, MS 9161, Livermore, CA, 94550 USA
PH: +1 (925) 294-2872

†Present affiliation: University of California, Santa Barbara, Department of Materials Science, Santa Barbara, CA 93117

above. These results will be reported in a forthcoming publication (c.f. Ref. [1]). We also consider six additional samples that were exposed to varying plasma fluences, which comprise data set "B." The surface morphologies of these specimens were already reported in a previous paper and compared with an atomistically-informed continuum scale model (discussed in Ref. [2].) In this case, each sample was heated to 840 ± 20 °C. The surface evolution largely mimics the behavior observed with varying temperature, where the initial roughening is coupled with near-surface bubble growth and bursting. As the exposure time increases, a network of 50 nm diameter nano-tendrils emerges, much like the temperature dependence series.

Data sets "C" and "D" were not intended to systematically explore dependencies on exposure conditions. Instead, the experimental parameters were selected with the goal of producing a thick W nanostructure layer for permeation and recrystallization studies. The exposures included in data set D are described in detail in a recent publication by Wong et al. [3]. A representative top-view image of the specimen from data set C is included in Fig. S2. This specimen was punched from rolled polycrystalline W foil, and thus had a much different grain structure in comparison to the ITER-grade material used for all the other samples in this study. We did not note any obvious difference in the structure of the nano-tendrils due to these differences. In the case of data set D, all the exposure conditions were held constant. Unfortunately, unlike in the other data sets, we had difficulty in attaining consistent fuzz growth between exposures (in principle they should all be nearly the same). Even though different thicknesses were attained, all the ellipsometry data matched up satisfactorily with the basic trend mapped out in Fig. 3.

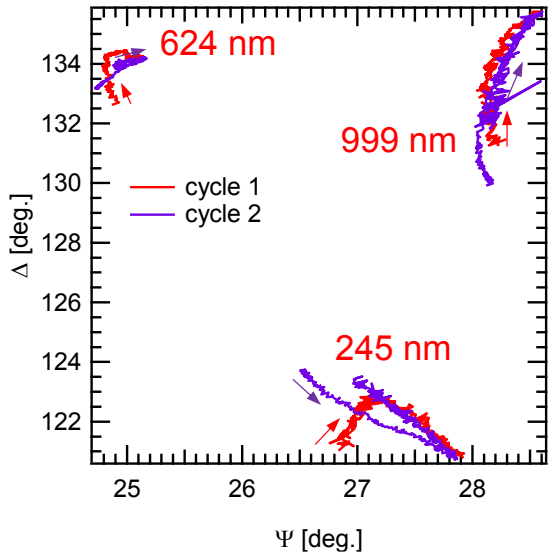

Fig. S1: Variation of Δ and Ψ during sample heating up to 900 °C from 25 °C and cooling afterward. Two heating cycles are shown here, for three discrete wavelengths (245 nm, 624 nm, and 999 nm.) The arrows indicate the starting point and initial direction of each trajectory

Regarding the interpretation of the ellipsometry results, one consideration for the thicker nanostructures is the penetration depth of the incident light. This would likely depend on the density of the fuzz layer and the degree to which light is scattered within it. More modelling is needed to determine the maximum thickness that can be detected, though even at fluences up to 10^{25} m^{-2}, we continue to see changes in Δ and Ψ in our ellipsometry data with increasing fluence. With proper calibration against microscopy images, it is plausible that the technique would continue to provide useful data at higher fluences. The main consequence would be diminished sensitivity. For example, from Fig. 3 in the main article, the growth of a tungsten fuzz layer that is 400 nm thick produces a change in Δ of 100° compared with the pristine surface. However, an additional 500 nm of growth (resulting in a total nanostructure layer thickness of 900 nm) causes only an additional 20° change in

Δ. For extremely thick nanostructures, only the top few microns may contribute to the measured signal, it is possible that this effect may need to be taken into consideration when attempting to model the ellipsometry data. Given that most of the nanostructure layers considered here are thinner than this (< 1 μm), this would only affect a small number of samples included in this study.

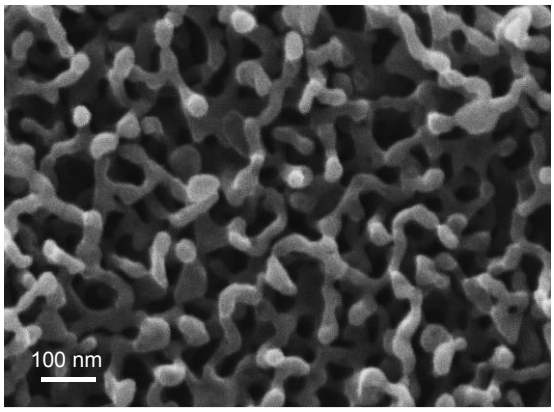

Fig. S2: "Top view" HIM image of W nanotendrils formed following He plasma exposure. The surface morphology depicted here is representative of specimens from data set "C". Exposure conditions: T_{sample} = 900 °C; E_{ion} = 92 eV; $\Gamma_{ion} = 4.0\times10^{20}$ m^{-2} s^{-1}, $\Phi_{ion} = 7.2\times10^{24}$ m^{-2}.

Table S1: Detailed set of ex-situ exposure conditions for low energy He^+ exposures

data set ID	# of samples	Comments
A	9	Sample temperature varied between 472 – 937 °C. Exposure conditions: E_{ion} = 92 eV; $\Gamma_{ion} = 4.0\times10^{20}$ m^{-2} s^{-1}; $\Phi_{ion} = 7.2\times10^{24}$ m^{-2}. Material: ITER-grade W Temperature data points: T_{sample} = 472 °C, 546 °C, 658 °C, 720 °C, 786 °C, 815 °C, 848 °C, 889 °C, and 937 °C
B	6	Ion fluence varied between $\Phi_{ion} = 5.0\times10^{23} – 1.2\times10^{25}$ m^{-2}. Exposure conditions: T_{sample} = 840 °C; E_{ion} = 92 eV; $\Gamma_{ion} = 2.7\times10^{20}$ m^{-2} s^{-1}. Results reported in Ref. [26]. Material: ITER-grade W Fluence data points: $\Phi_{ion} = 5.0\times10^{23}$ m^{-2}, 1.2×10^{24} m^{-2}, 2.7×10^{24} m^{-2}, 4.5×10^{24} m^{-2}, 6×10^{24} m^{-2}, 1.2×10^{25} m^{-2}
C	1	Exposure conditions: T_{sample} = 900 °C; E_{ion} = 92 eV; $\Gamma_{ion} = 4.0\times10^{20}$ m^{-2} s^{-1}, $\Phi_{ion} = 7.2\times10^{24}$ m^{-2}. Material: rolled polycrystalline W foil
D	5	Exposure conditions: T_{sample} = 840 °C; E_{ion} = 92 eV; $\Gamma_{ion} = 4.0\times10^{20}$ m^{-2} s^{-1}; $\Phi_{ion} = 8.6\times10^{24}$ m^{-2}. Material: ITER-grade W. Results reported in Ref. [31].

REFERENCES

[1] R. D. Kolasinski, C. -S. Wong, A. Engel, J. A. Whaley, F. I. Allen, and D. A. Buchenauer, (in preparation.)

[2] D. Dasgupta, R. D. Kolasinski, R. W. Friddle, L. Du, D. Maroudas, and B. D. Wirth, *Nucl. Fusion* **59**, 086057 (2019).

[3] C. -S. Wong, J. A. Whaley, T. Wada, S. Harayama, Y. Oya, and R. D. Kolasinski, *Nucl. Mater. Energy* **22**, 100730 (2020).